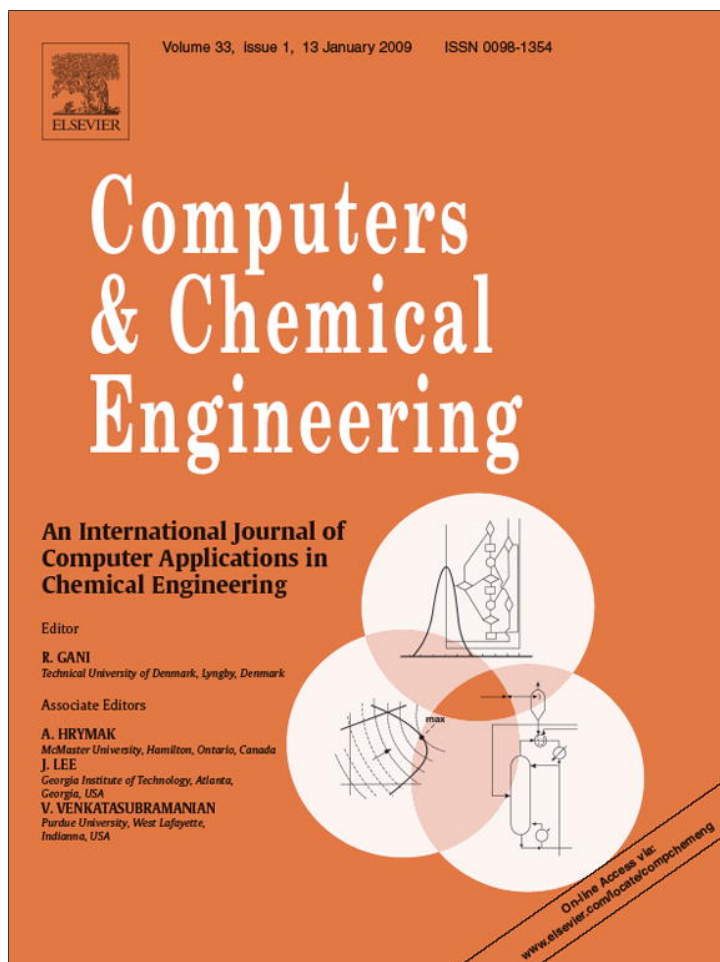


Provided for non-commercial research and education use.
Not for reproduction, distribution or commercial use.



This article appeared in a journal published by Elsevier. The attached copy is furnished to the author for internal non-commercial research and education use, including for instruction at the authors institution and sharing with colleagues.

Other uses, including reproduction and distribution, or selling or licensing copies, or posting to personal, institutional or third party websites are prohibited.

In most cases authors are permitted to post their version of the article (e.g. in Word or Tex form) to their personal website or institutional repository. Authors requiring further information regarding Elsevier's archiving and manuscript policies are encouraged to visit:

<http://www.elsevier.com/copyright>



Contents lists available at ScienceDirect

Computers and Chemical Engineering

journal homepage: www.elsevier.com/locate/compchemeng

Global modeling and simulation of a three-phase fluidized bed bioreactor

Mauren Fuentes^{a,b}, Miguel C. Mussati^{a,c}, Nicolás J. Scenna^{a,c}, Pío A. Aguirre^{a,d,*}^a INGAR - (CONICET-UTN), Avellaneda 3657 (3000) Santa Fe, Argentina^b Depto de Ciencias Básicas - UTN FRSE, Lavalse 610 (3000) Santa Fe, Argentina^c CAIMI-UTN FRR, Zeballos 1341 (2000) Rosario, Argentina^d Facultad de Ing. Qca, UNL, Santiago del Estero 2829 (3000) Santa Fe, Argentina

ARTICLE INFO

Article history:

Received 1 June 2006

Received in revised form

11 September 2008

Accepted 5 October 2008

Available online 17 October 2008

Keywords:

Dynamic modeling and simulation

Three-phase systems

Fluidized bed bioreactors

Wastewater treatment

ABSTRACT

The main purpose of this paper was to present a heterogeneous model of a three-phase solid–liquid–gas system to investigate the hydrodynamics and biological behavior and the system performance of anaerobic fluidized bed reactors (AFBRs). The Anaerobic Digestion Model No. 1 (ADM1) was selected to describe the substrate degradation scheme and was applied to a biofilm system. Global modeling of AFBRs involves differential mass and momentum balance equations for the three phases, differential mass balance equations for phase components, and algebraic equations to compute the biochemical and physico-chemical processes that take place in the bioreactor. A one-dimensional (axial) dynamic model was proposed, and different phase flow patterns were analyzed. Simulation results of a case study based on a feed with a low substrate concentration (1 g of chemical oxygen demand, COD, per liter) are shown. As first approach, biochemical transformations are assumed to occur only in the fluidized bed zone but not in the free-support material zone. A sensitivity analysis of simulation results related to model parameters with high uncertainty such as specific biofilm detachment rate, liquid–gas mass transfer coefficient, and particle density and diameter was performed. A second approach based on model extension to the two-phase non-fluidized zone allowed evaluating the effect of substrate consumption by suspended biomass in the free-bioparticles zone. A decrease in the biofilm concentration up to 3.6% and thus, a decrease in the COD removal efficiency was predicted. However, some factors involving the biofilm detachment rate, reactor design characteristics and substrate residence time need to be analyzed for each specific case. The implementation of this modeling approach resulted in more programming effort and CPU time than the first one. A key feature of the model is the simultaneous prediction of phases and components dynamics, including the effect of biofilm growth in the fluidization characteristics and interaction among them in both hydrodynamic and biological transients.

© 2008 Elsevier Ltd. All rights reserved.

1. Introduction

Stringent norms and regulations for discharging contaminating streams into natural receiving water bodies push industries to treat wastewaters with high efficiency using reliable treatment systems. In the last decades anaerobic processes have been considered a mature technology for processing a wide spectrum of wastewaters, mainly those having high organic contaminating load.

On the other hand, the fluidized bed reactor is one of the most widely used high-rate systems. This reactor type retains

high attached biomass concentration on an inert support material, presents smaller pressure drop than fixed bed systems, shows no bed-clogging problems, demands small reactor volume and determines low external mass transport resistance when being compared to other reactor configurations. However, some practical aspects need to be addressed. Due to the slow growth rate of the anaerobic consortium compared to the aerobic growth, anaerobic systems require long periods for starting up and recovering an efficient operation regimen after a sudden increase of the organic load due to a perturbation of either the inlet flow rate or contaminating concentration.

When the disturbance is on the inlet flow rate, the system hydrodynamics is significantly affected; whereas when a disturbance on the influent organic concentration occurs, the biological process rates govern the transient behavior of the system. However, the biological process rates affect the system hydrodynamics since variations on the biofilm concentration modify the density of the

* Corresponding author at: INGAR -Instituto de Desarrollo y Diseño- Avellaneda 3657 (3000) Santa Fe, Argentina. Tel.: +54 342 4534451; fax: +54 342 4553439.

E-mail addresses: mfuentes@santafe-conicet.gov.ar (M. Fuentes), mmussati@santafe-conicet.gov.ar (M.C. Mussati), nscenna@santafe-conicet.gov.ar (N.J. Scenna), paguir@santafe-conicet.gov.ar (P.A. Aguirre).

Nomenclature

A	area
D, d	diameter
D_z	axial dispersion coefficient
F	force
g	gravity
H	height
I_{COD}	index g COD mol ⁻¹
k	specific rate coefficient
$k_L a$	liquid–gas mass transfer coefficient
K_H	Henry's Law coefficient
N	number
n	expansion coefficient
P, p	pressure
Q	flow rate
R	homogeneous reaction rate
Re	Reynolds number
S	soluble species concentration
T	mass transfer and transport process rate at the interface
t	time
U	velocity
V	volume
W	particle load
X	biomass concentration or non-soluble species concentration
X_c	particulate material concentration
z	axial direction

Greek symbols

δ	biofilm thickness
ε	holdup (volumetric fraction)
μ	specific growth rate (Table 3), viscosity
v_{st}	gas molar volume
ξ	holdup in two-phase pseudo-system
ρ	density
ω	specific energy dissipation rate
ϕ	mass or molar concentration
-	axial mean value

Subscripts

a	active (biomass)
B	gas bubble
bh	biomass hydrolysis
bp	bioparticle
c	reactor column
d	biomass death
dis	disintegration of particulate material
E	biofilm detachment
E_s	relative to the force acting on fluidized particles in the axial direction
F	film (wet density)
f	feed
G, g	gas, gravity (force)
H	particulate material hydrolysis
I	interaction (force)
i	phase component index
j	biochemical and physico-chemical process index
k	phase index
L, l	liquid
na	non-active (biomass)

o	inlet, initial or static bed condition
p	particle, pressure (force)
r	recycle
S	solid
T	total
t	terminal

support particles and, consequently, their fluidization characteristics. Indeed, fluidization characteristics such as fluidized bed height and phase holdups (volume fractions) are critical because of their influence on residence time, specific biofilm superficial area in the biologically active zone, reactor size, mass transfer and biofilm detachment rate. Thus, a main concern in fluidized bed biofilm reactor modeling is to compute hydrodynamic phenomena and their interaction with the biological variables. Then, detailed three-phase models considering hydrodynamics of solid–liquid–gas system, the biofilm system and the anaerobic digestion process itself are required to capture both the biological and hydrodynamic transient behavior of the bioreactor.

Among all the former works (Abdul-Aziz & Asokelar, 2000; Bonnet, Dochain, & Steyer, 1997; Diez Blanco, García Encina, & Fdez-Polanco, 1995; Huang, Yan, & Wu, 2000; Yu & Rittmann, 1997) concerning AFBR modeling, few of them deal with the computational fluid dynamics approach for two-phase flow. This study continues on from the previous works accomplished by Bonnet et al. (1997) but now taking into account three phases, including an anaerobic digestion model applied to a multispecies biofilm system, and combining the dynamics of the biological and hydrodynamic processes. The main objectives of this paper are: (a) to present a heterogeneous model of an anaerobic fluidized bed reactor considered as a three-phase solid–liquid–gas system, assuming parameter values accepted in literature; (b) to use the proposed model for performing a phenomenological analysis of both biological and hydrodynamic behaviors of the system for a defined case study. Rigorous dynamic momentum and mass balances for solid, liquid and gas phases characteristic of anaerobic methanogenic fluidized bed biofilm reactors are solved to determine the force, velocity and holdup profiles of each phase, the substrate and product concentration profiles, the system pH, and off-gas composition and flow rate dynamics.

The paper is organized as follows: In Section 2, the structure and main equations of the mathematical model are presented. Computational aspects including numerical aspects and the model solution strategy are described in Section 3. Simulation results describing the main process variables related to the system hydrodynamics and the biological processes for a case study assuming different control volumes are presented in Section 4. Finally, conclusions are drawn in Section 5.

2. Mathematical model

In anaerobic digestion, complex organics such as carbohydrates, proteins, and lipids are first hydrolyzed by enzymes to sugars, amino acids, and fatty acids, respectively. These intermediate products are then degraded by acidogens to volatile fatty acids (VFAs), which are further degraded by acetogens forming acetate, carbon dioxide (CO₂), and hydrogen (H₂). Last, acetate and H₂/CO₂ are converted by acetoclastic and H₂-utilizing methanogens, respectively, to methane (CH₄). Acidogens grow faster and are less sensitive to pH variation than acetogens and methanogens. This usually results in the accumulation of organic acids and pH decreases, leading to the suppression of methanogenic activity and, in some cases, even

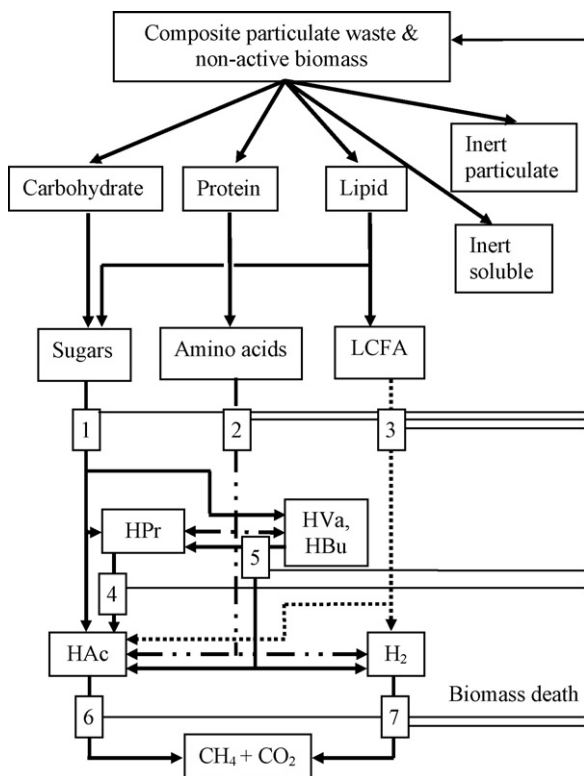


Fig. 1. Anaerobic degradation steps for ADM1 (Batstone et al., 2002): (1) acidogenesis from sugars (glucose); (2) acidogenesis from amino acids; (3) acetogenesis from long chain fatty acid (LCFA); (4) acetogenesis from propionate (HPr); (5) acetogenesis from butyrate (HBU) and valerate (HVa); (6) acetoclastic methanogenesis; and (7) hydrogenotrophic methanogenesis.

to process failure (Angelidaki, Ellegaard, & Ahring, 1999; Batstone, Keller, & Blackall, 2004; Yu & Fang, 2003). Thus, an anaerobic digestion scheme has to be adequately described by the biochemical and physico-chemical processes. In this work, Anaerobic Digestion Model No. 1 (ADM1) proposed by Batstone et al. (2002) has been used. Fig. 1 represents the degradation steps and microorganism trophic groups assumed in ADM1.

Application of the ADM1 to a biofilm system requires the modeling of the interaction between suspended and attached biomass. Fig. 2 represents the main biochemical (growth-uptake, death, hydrolysis and detachment) processes. As microorganisms attach

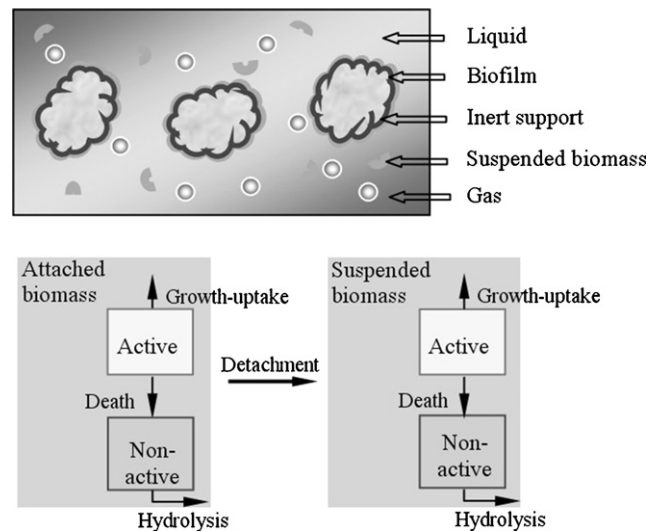


Fig. 2. Main biochemical processes and interactions between suspended and attached biomass.

on the bare support and develop forming biofilm, a bioparticle model is required to model an AFBR.

So, the AFBR is modeled as a three-phase gas–solid–liquid system (see Fig. 4). The solid phase consists of the inert support particles and the (active and non-active) attached biomass (biofilm). In the multispecies biofilm model, biomass is considered as a continuum; that is, biomass is mathematically characterized by average quantities such as the concentration of microbial species. The liquid phase is composed by the chemical species in solution (substrates, products, enzymes, ions, and water) and (active and non-active) suspended biomass. The gas phase is formed by the gaseous products from degradation stages.

Definition of the control volume and time–space domains of process variables is needed to model hydrodynamics and phase interactions. Then, fluidization characteristics (phase holdups and velocities) can be calculated from phase mass and momentum balances.

The global model structure is represented in Fig. 3.

2.1. Mass and momentum balance equations

Fig. 4 represents the main streams in the fluidized bed reactor and the three-phase system assumed to model the AFBR. A

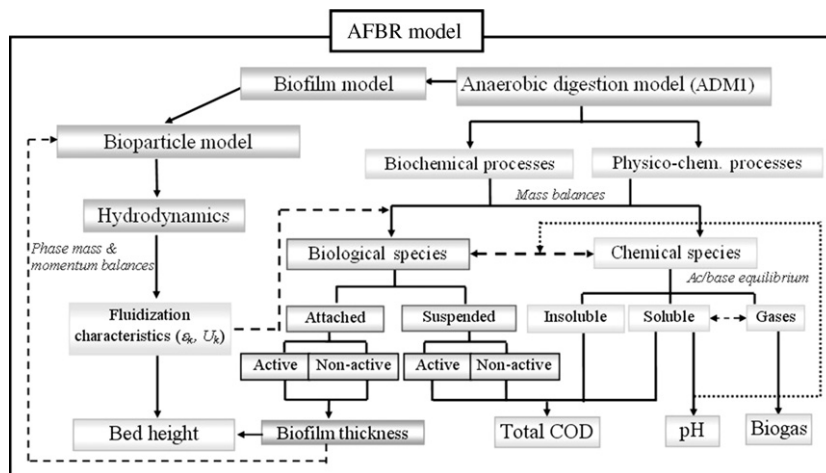


Fig. 3. Anaerobic fluidized bed reactor (AFBR) model structure.

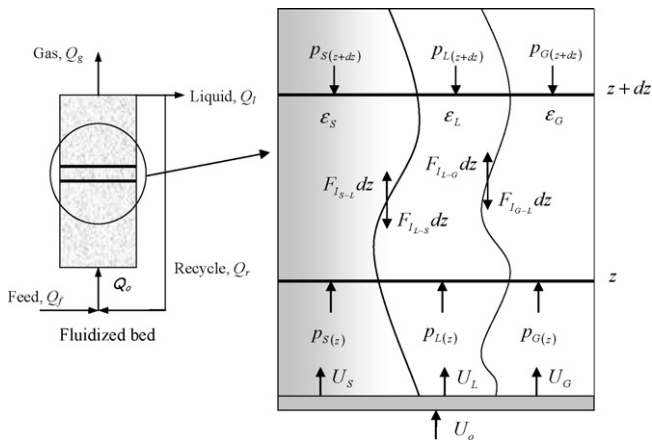


Fig. 4. Three-phase solid-liquid-gas system assumed to model the AFBR.

general axial dispersive model is used to represent the phase behavior.

The relationship among the phase volume fractions (holdups) ϵ_k has to verify:

$$\sum_k \epsilon_k = 1 \quad (1)$$

where k indicates liquid ($k=L$), solid ($k=S$) and gas ($k=G$) phases.

Eqs. (2) and (3) represent the mass and momentum balances for phase k , respectively:

$$\partial \frac{\epsilon_k \rho_k}{\partial t} = -\partial \frac{\epsilon_k \rho_k U_k}{\partial z} + \frac{\partial}{\partial z} \left(D_{zk} \partial \frac{\epsilon_k \rho_k}{\partial z} \right) + \sum_{i,j} T_{ik} \quad (2)$$

where ρ_k and U_k represent the intrinsic density and velocity of phase k , respectively. $\sum_{i,j} T_{ik}^j$ represents the sum of all mass transfer and transport process rates j at the interface between phase k and the other two phases, in which all components i are involved.

$$\partial \frac{\epsilon_k \rho_k U_k}{\partial t} = -\partial \frac{\epsilon_k \rho_k U_k^2}{\partial z} + \frac{\partial}{\partial z} \left(D_{zk} \partial \frac{\epsilon_k \rho_k U_k}{\partial z} \right) + F_{gk} + F_{pk} + F_{lk} \quad (3)$$

where F_{gk} , F_{pk} and F_{lk} represent the contribution of the gravity, pressure and interaction forces, respectively (Foscolo & Gilibaro, 1987; Hatta, Fujimoto, Isobe, & Kang, 1998). Force expressions for momentum balances are summarized in Table 1.

In Table 1, ξ_k represents the volume fraction of each phase in the two-phase pseudo-system where the interaction force takes place. Note that the interaction force between solid and gas phases has been neglected. F_{E_s} is the force acting on fluidized particles in the axial direction due to an approaching particle concentration perturbation, and it is an additional force for the solid phase not represented in Eq. (3).

Table 1
Force expressions for momentum balances.

Force expressions	
$F_{gk} = -\epsilon_k \rho_k g$, $k = S, L, G$	
$F_{pk} = -\epsilon_k \frac{\partial p}{\partial z}$, $\frac{\partial p}{\partial z} = -g \sum_k \epsilon_k \rho_k$, $k = S, L, G$	
$F_{l-s} = -F_{l-s} = \xi_s (\rho_p - \rho_L) g \left(\frac{U_0 - U_s}{U_t} \right)^{4.8/n} \xi_L^{-3.8}$	
$F_{l-g} = -F_{l-g} = \frac{36 \xi_G \mu_L (U_G - U_L)}{d_b^2}$	
$F_{E_s} = -3.2 d_{bp} g \xi_s (\rho_s - \rho_L) \frac{\partial \xi_s}{\partial z}$	

Table 2
Homogeneous reaction rates and mass transfer and transport process rates ($\sum_j R_{ik}^j + \sum_j T_{ik}^j$) involved in mass balance equations for component i .

ϕ_{ik}^a	$\sum_j R_{ik}^j + \sum_j T_{ik}^j$	i
X_{la}^S	$\epsilon_S [\mu_i X_{la}^S - k_d X_{la}^S - k_E \omega X_{la}^S]$	17–23
X_{ina}^S	$\epsilon_S [k_d X_{la}^S - k_{bh} X_{ina}^S - k_E \omega X_{ina}^S]$	17–23
X_{la}^L	$\epsilon_L [\mu_i X_{la}^L - k_d X_{la}^L] + \epsilon_S k_E \omega X_{ina}^S$	17–23
X_{ina}^L	$\epsilon_L [k_d X_{la}^L - k_{bh} X_{ina}^L] + \epsilon_S k_E \omega X_{ina}^S$	17–23
S_i	$\sum_{j=5-12} v_{i,j} \mu_j (\epsilon_S X_{ja}^S + \epsilon_L X_{ja}^L) + \sum_{j=2-4} v_{i,j} k_{Hid,j} \epsilon_L X_j$	1–7,11
S_i	$\sum_{j=5-12} v_{i,j} \mu_j (\epsilon_S X_{ja}^S + \epsilon_L X_{ja}^L) - \epsilon_L (k_L a)_i (S_i - I_{COD} K_{H,i} P_{gas,i})$	8–10
X_i	$\sum_{j=2-4} v_{i,j} k_{Hid,j} \epsilon_L X_j + v_{i,j=1} k_{dis} \epsilon_L X_C$	12,14–16,24
X_C	$-k_{dis} \epsilon_L X_C + k_{dis} \sum_{j=13-19} (\epsilon_S X_{ja}^S + \epsilon_L X_{ja}^L)$	13
$P_{gas,i}$	$v_{st} P_{gas,T} \epsilon_L (k_L a)_i (S_i / I_{COD} - K_{H,i} P_{gas,i})$	8–10

^a Mass balances of phase components are expressed in grams of chemical oxygen demand per liter per day ($g\ COD\ L^{-1}\ d^{-1}$), except for inorganic carbon and nitrogen ($mol\ L^{-1}\ d^{-1}$) and gas phase components ($atm\ L^{-1}\ d^{-1}$).

The mass balance equation for a component i of concentration ϕ_{ik} in phase k is

$$\partial \frac{\epsilon_k \phi_{ik}}{\partial t} = -\partial \frac{\epsilon_k \phi_{ik} U_k}{\partial z} + \frac{\partial}{\partial z} \left(D_k \partial \frac{\epsilon_k \phi_{ik}}{\partial z} \right) + \sum_j R_{ik}^j + \sum_j T_{ik}^j \quad (4)$$

where $\sum_j R_{ik}^j$ is the sum of all homogeneous reaction rates j , and $\sum_j T_{ik}^j$ is the sum of all mass transfer and transport process rates j through interfaces, where component i is involved.

2.1.1. Reaction, mass transfer and transport process rates

The terms $\sum_j R_{ik}^j + \sum_j T_{ik}^j$ are related to biochemical (uptake, growth, death, hydrolysis and detachment) and physico-chemical processes. Expressions to calculate them are summarized in Table 2. In this work, only external mass transfer processes have been modeled. No mass transfer limitations in the biofilm and liquid film are assumed. The concentration inside the biofilm is considered a time function and has the same value throughout the biofilm. A description of variables (i) and processes (j) involved in the anaerobic digestion model is presented in Table 3.

Table 3
Variables (i) and processes (j) taken into account in the anaerobic digestion model.

Variable	Description	i	Processes	j
X_C	Composite	13	Disintegration	1
X_{CH}	Carbohydrate	14	Carbohydrate hydrolysis	2
X_p	Protein	15	Protein hydrolysis	3
X_{Li}	Lipid	16	Lipid hydrolysis	4
X_I	Inert particulate	24	Glucose uptake	5
S_I	Inert soluble	12	Amino acid uptake	6
S_{Gl}	Glucose	1	LCFA uptake	7
S_{AA}	Amino acid	2	Valerate uptake	8
S_{LCFA}	LCFA	3	Butyrate uptake	9
S_{HVa}	Valerate	4	Propionate uptake	10
S_{HBu}	Butyrate	5	Acetate uptake	11
S_{HPr}	Propionate	6	H ₂ uptake	12
S_{HAc}	Acetate	7	X_{GL} decay	13
S_{H2}	Hydrogen	8	X_{AA} decay	14
S_{CH4}	Methane	9	X_{LCFA} decay	15
S_{IC}	Inorganic carbon	10	X_{C4} decay	16
S_{IN}	Inorganic nitrogen	11	X_{Pr} decay	17
X	Biomass	17–23	X_{Ac} decay	18
			X_{H2} decay	19
			H ₂ mass transfer	T8
			CH ₄ mass transfer	T9
			CO ₂ mass transfer	T10

Table 2 includes the terms $\sum_j R_{ik}^j + \sum_j T_{ik}^j$ for active (*a*) and non-active (*na*) biological species in solid (X_i^S) and liquid (X_i^L) phases, soluble (S_i) and insoluble chemical species (X_i), particulate material (X_C), and gas phase components. v_{ij} is the biochemical rate coefficient of component *i* related to degradation stage *j*. μ , k_d , k_E and k_{bh} are the specific rates of microbial growth and death, biofilm detachment and hydrolysis of biomass, respectively. Finally, k_{Hid} is the specific hydrolysis rate. In Table 2, the terms $\sum_j R_{ik}^j + \sum_j T_{ik}^j$ corresponding to soluble substrates produced during biopolymer hydrolysis ($S_{i=1-7,11}$) and soluble substrate and products transferred to gas phase ($S_{i=8-10}$) have been distinguished.

Specific growth and death rates are assumed to be the same for suspended and attached biomass. In addition, the specific biomass hydrolysis rate is the same for all species. Since non-active biomass is considered as particulate material subjected to disintegration and hydrolysis (see Fig. 1), k_{bh} is equal to the specific disintegration rate of particulate material k_{dis} .

The biofilm process model is coupled to the system hydrodynamic model through the biofilm detachment rate r_E which is modeled as a first-order function on the specific energy dissipation rate ω , and mass concentration of each attached microbial species *i* (Table 2):

$$r_{E_i} = \varepsilon_S k_E \omega X_i^S \quad (5)$$

Specific energy dissipation rate ω was used by Huang and Wu (1996) to study the biofilm thickness distribution in fluidized bed reactors, assuming that the erosion effects on the biofilm surface are related to this parameter that is calculated as

$$\omega = U_o \left(-\frac{\partial p}{\partial z} \right) \quad (6)$$

where U_o is the superficial fluid velocity at the reactor column inlet.

Specific detachment rate k_E is assumed to be the same for all biological species.

ADM1 assumes H_2 , CO_2 and CH_4 as components of the gas phase. Here, water vapor has been considered too. The liquid–gas mass transfer is modeled assuming ideal gas behavior and constant gas phase total pressure ($p_{gas,T} = p_{gas,H_2O} + p_{gas,CH_4} + p_{gas,CO_2} + p_{gas,H_2}$). The mass balance for gas phase component *i* is expressed as a function of its partial pressure $p_{gas,i}$ (Table 2). $K_{H,i}$ and $(k_L a)_i$ represent Henry's Law coefficient and the liquid–gas mass transfer coefficient of gas phase component *i*, respectively. v_{st} is the gas molar volume. Water vapor pressure p_{gas,H_2O} is calculated by an Antoine-type equation.

The physico-chemical model includes the system charge balance (electroneutrality condition) for calculating pH. It involves mass balance equations for total concentration of volatile fatty acids (VFAs: acetic, propionic, butyric and valeric), inorganic carbon, inorganic nitrogen, phosphate, "other anions", and "other cations". The last three chemical species are not represented in Tables 2 and 3, but they are state variables that do not contribute to bioreaction and transfer processes ($\sum_j R_{ik}^j + \sum_j T_{ik}^j = 0$) and differential mass balance equations for these liquid phase components are stated too.

The biochemical rate equation matrix and the relationships of the acid–base equilibrium model are extracted from Batstone et al. (2002), and are not here included due to space restrictions.

2.2. Bioparticle model. Influence of the biofilm growth on the bed porosity and height

Homogeneous biofilm distribution on support particles, constant density and diameter of support particles, constant wet

biofilm density and spherical geometry are assumed for the bioparticle model (Abdul-Aziz & Asokelar, 2000). The number of support particles (i.e. the number of bioparticles) is assumed constant, and these are homogeneously distributed within the entire reactor.

As derived from model assumptions, the bioparticle diameter d_{bp} and density ρ_{bp} (equal to the solid phase density ρ_s), and the volumetric ratio between biofilm and material support *x* can be calculated as

$$d_{bp} = d_p + 2\delta \quad (7)$$

$$\rho_{bp} = \frac{\rho_p + x\rho_F}{1+x} \quad (8)$$

$$x = \left(\frac{d_{bp}}{d_p} \right)^3 - 1 \quad (9)$$

where δ is the biofilm thickness, d_p and ρ_p are the mean diameter and density of support particles, respectively; and ρ_F is the wet biofilm density.

From the mass balance in the solid phase and the bioparticle model described above, the following relationship between the biofilm thickness δ and the total (active and non-active) attached biomass concentration X_T^S can be derived:

$$X_T^S = \rho_F \left[1 - 1 / \left(1 + \frac{2\delta}{d_p} \right)^3 \right] \quad (10)$$

In bioreactors, the solid holdup varies during the biological transient due to the ongoing microbiological processes: growth, death, detachment and hydrolysis of biomass. Gas holdup also varies but its contribution is generally negligible compared to the solid and liquid holdups in anaerobic reactors. Even when these microbiological processes cause a time variation of bed porosity, this change is sufficiently slow compared to those caused by a hydrodynamic transient. A biofilm thickness increase causes an increase in the total height *H* of the fluidized bed.

Eq. (11) is used to calculate the bed height. It is based on the definition of solid holdup in the control volume of the entire reactor, and is an integrated entity since properties vary in the axial direction of the bed. Although support particles are homogeneously distributed, the biofilm thickness, and thus, the bioparticle diameter vary with time and in the axial direction of the bed. Since the solid holdup $\varepsilon_s(z, t)$ can be interpreted as the volume fraction of the total bioparticle volume in the volume $dV = A_c dz$; from an overall material balance in the reactor unit, the height (*H*) of the fluidized bed can be calculated as follows:

$$H = \frac{1}{A_c} \frac{N_{bp} \bar{V}_{bp}}{\varepsilon_S} = \frac{1}{A_c} \frac{N_{bp} \left[\frac{1}{H} \int_z V_{bp} dz \right]}{\left[\frac{1}{H} \int_z \varepsilon_S dz \right]} \quad (11)$$

where V_{bp} and N_{bp} are the bioparticle volume ($V_{bp} = \pi(d_p + 2\delta)^3/6$) and the number of bioparticles ($N_{bp} = W/\rho_p V_p = W/\rho_p(\pi d_p^3/6)$), respectively. Finally, Eq. (11) can be rewritten as follows:

$$H = \frac{W}{\rho_p A_c \left[\frac{1}{H} \int_z \varepsilon_S dz \right]} \left[\frac{1}{H} \int_z \left(1 + \frac{2\delta}{d_p} \right)^3 dz \right] \quad (12)$$

where *W* and A_c are the initial particle load and the column cross section area, respectively.

Liquid and gas phase densities can be assumed as time- and space-invariants in biological and hydrodynamic time horizons. Solid density (ρ_s) is a function of the biofilm thickness, which can be considered as an invariant in hydrodynamic transients but not in biological transients.

These simplifying assumptions were introduced to make the model workable, although they do not completely reflect reality.

Revision of these assumptions to more realistic ones (e.g. introduction of the size distribution of particles, variable density of biofilm with time, and characteristics of support particles such as shape, roughness, and material porosity) will be the next step for model refinement.

2.3. Model parameters and constants

The global model has to be able to represent dynamics of different processes. Well-known and accepted parameter values have been assumed in the proposed model for each sub-system. However, responses of such model show general tendencies of process variables. An exhaustive compilation of experimental data needs to be carried out to obtain accurate information to simulate the experimental scenarios (Fuentes, Aguirre, Scenna, & Mussati, 2007). In practice, operating disturbances and unexpected bioreactor failures increase uncertainty on bioreactor performance and have to be included in the simulation schedule for model calibration (parameter estimation). Therefore, an extensive analysis is needed to determine which of these events have a significant influence on parameter estimation. These aspects were pointed out in a previous work for calibrating an AFBR model (Fuentes, Aguirre, Scenna, & Mussati, 2008).

2.3.1. Biochemical and physico-chemical parameters

Microorganism growth kinetic expressions and kinetic and physico-chemical parameters are taken from the ADM1 original paper (Batstone et al., 2002). Parameters for mesophilic temperature at high rate operation conditions are used. Specific detachment rate k_E must be estimated from experimental data. From results presented by Mussati, Fuentes, Aguirre, & Scenna (2005a) and recently, by Fuentes et al. (2008), a value for $k_E = 2.24 \times 10^{-10} \text{ m s}^2 \text{ kg}^{-1}$ is here used. The liquid–gas mass transfer coefficient of gas phase component $(k_L a)_i$ is assumed as 100 d^{-1} for all components of gas phase (Graef & Andrews, 1973).

2.3.2. Hydrodynamic parameters

In bioreactors, hydrodynamic parameters such as the terminal settling velocity U_t and the expansion coefficient n are functions of the biofilm thickness. Researchers, such as Nicolella, van Loosdrecht, & Heijnen (2000), Yu and Rittmann (1997), Setiadi (1995), Mulcahy and Shieh (1987), Thomas and Yates (1985), Hermanowicz and Ganzarczyk (1983), Ngian and Martin (1980), have studied the effects of biofilm accumulation on parameters U_t and n in fluidized bed reactors. Most of them reported their results from correlations originally derived for rigid particles that were modified for biofilm system applications. In a previous work (Fuentes et al., 2008), a sensitivity analysis of correlations proposed by these authors for estimation of parameters U_t and n was presented. The aim was to show the dispersion of results using the most quoted correlations. However, they have been mainly applied to aerobic biofilm systems, and seem to be less appropriate for anaerobic systems than the original equation of Richardson and Zaki (1954) (Eq. (14)), quite used to calculate n in most works focused on anaerobic fluidized bed reactors, and Eq. (13) provided by Foscolo, Giliardo, & Waldarm (1983) to calculate U_t . These correlations are valid for the range of Reynolds number (Re_t) here investigated.

$$U_t = \frac{-17.3\mu_L + \left[299.29\mu_L^2 + 1.344gd_{bp}^3\rho_L(\rho_S - \rho_L)\right]^{0.5}}{0.672d_{bp}\rho_L} \quad (13)$$

$$n = 4.4Re_t^{-0.1}, \quad 1 < Re_t < 500, \quad Re_t = \frac{U_t d_{bp} \rho_L}{\mu_L} \quad (14)$$

Since an axial dispersive model is proposed to describe the phase behavior, expressions to calculate phase dispersion coefficients are needed. Several correlations were proposed to compute the axial dispersion coefficient for the liquid phase (Muroyama & Fan, 1985), but little information is available for gas and solid phases. In this work, the correlation given by Kim and Kim (1983) is used for calculating the axial dispersion coefficient of the liquid phase D_{zL} :

$$\frac{d_p \varepsilon_L U_L}{D_{zL}} = 20.19 \left(\frac{d_p}{D_c}\right)^{1.66} \left(\frac{\varepsilon_L U_L}{\varepsilon_L U_L + \varepsilon_G U_G}\right)^{1.03} \quad (15)$$

where D_c is the reactor column diameter.

A sensitivity analysis of the model predictions related to gas and solid phase dispersion coefficients is presented in Section 4.

2.4. Initial and boundary conditions

As first approach, biochemical transformations are assumed to occur only in the fluidized bed zone but not in the free-support material zone. The nature of anaerobic biochemical processes makes initial (IC) and boundary (BC) conditions quite different from the traditional ones found in the literature for three-phase systems.

Ideal perfect mixture hypothesis is considered as initial condition. For hydrodynamic variables a static bed condition is assumed. Since the biofilm adsorption phenomenon is not modeled, low steady state concentration values are assigned as initial condition values for the biological and chemical species.

Danckwerts-type boundary conditions are considered at the reactor inlet ($z=0$) and outlet ($z=H$) for phase components. Since the solid is confined in the control volume, and the generated gas is separated from the multiphase stream in the upper part of the reactor column (see Fig. 4), boundary conditions for the components referred to the solid and gas phases are given by the no-flux condition at the reactor inlet. A general zero derivative boundary condition is considered at the reactor outlet. Table 4 summarizes IC and BCs for fluidization characteristics and phase components.

3. Computational aspects

The mathematical model was implemented and solved using the process modeling software tool gPROMS (Process Systems Enterprise Ltd). However, the equations are written in such a way that can be implemented in all computation environments suitable to handle this type of equations system.

The global AFBR model resulted in an integral–partial derivative and algebraic equation (IPDAE) system. An additional programming effort was needed since a “high-index” IPDAE system (index > 1) was verified. In high-index systems, the number of initial conditions that can be arbitrarily specified is lower than the number of differential variables; differential variables are not independent and numerical methods for solving ordinary differential equations can fail. In this work, this point could be solved by:

- rewriting the derivative of some variables as functions of other differential variables, i.e. diminishing the number of differential variables. For example, if $x1_{(z,t)} = f(x2_{(z,t)})$, the derivative of a function $\psi_{(z,t)} = x1_{(z,t)}x2_{(z,t)}$, calculated as $\partial \frac{\psi_{(z,t)}}{\partial t} = \left(\partial \frac{x2_{(z,t)}f(x2_{(z,t)})}{\partial t}\right)$, only needs an IC for $x2_{(z,t)}$, and $x1_{(z,t)}$ can be calculated as an algebraic variable; or
- directly assigning an IC for function $\psi_{(z,t)}$, so that $\psi_{(z,0)} = x1_{(z,0)}x2_{(z,0)} = \psi_0$.

Both alternatives provide the IPDAE system with consistent initial condition values.

Table 4
Initial and boundary conditions of AFBR model.

	IC ($t=0$)	BC ($z=0$)	BC ($z=H$)
Phase components	$\phi_{ik} = \phi_{ik_0}, \quad k = S, L, G$	$\partial \frac{\phi_{ik}}{\partial z} = 0, \quad k = S, G$	$\partial \frac{\phi_{ik}}{\partial z} = 0, \quad k = S, L, G$
Fluidization characteristics	$\varepsilon_S = \frac{W}{\rho_p A_c H_0}$	$\partial \frac{\phi_{iL}}{\partial z} = \frac{U_L}{D_{zL}} [\phi_{iL} - \phi_{iL}^*]$	$\partial \frac{\varepsilon_S}{\partial z} = 0$
	$U_S = 0$	$U_S = 0$	$U_S = 0$
	$\varepsilon_L = 1 - \varepsilon_S - \varepsilon_G$	$\partial \frac{\varepsilon_L}{\partial z} = 0$	$\partial \frac{\varepsilon_L}{\partial z} = 0$
	$U_L = \frac{U_0}{\varepsilon_L}$	$U_L = \frac{U_0}{\varepsilon_L}$	$\partial \frac{U_L}{\partial z} = 0$
	$\varepsilon_G = \varepsilon_{G_0}$	$\partial \frac{\varepsilon_G}{\partial z} = 0$	$\partial \frac{\varepsilon_G}{\partial z} = 0$
	$U_G = U_{G_0}$	$U_G = 0$	$\partial \frac{U_G}{\partial z} = 0$

Liquid phase concentrations at the reactor inlet ($z=0^-$) are calculated as $\phi_{iL}^* = \frac{1}{Q_0} [Q_f \phi_{iL_f} + Q_r \phi_{iL_{z=H}}]$, where ϕ_{iL_f} is the feed concentration and $\phi_{iL_{z=H}}$ is the recycle concentration (equal to the treated effluent concentration).

An axial dimensionless model was derived since gPROMS does not allow the straight calculation of moving boundary problems. Axial dimensionless length is defined as $z^* = z/H, 0 \leq z^* \leq 1$. The derivatives of the variables that are functions of z must be substituted as follows:

$$\frac{\partial}{\partial z} \rightarrow \frac{1}{H} \frac{\partial}{\partial z^*} \quad \text{and} \quad \frac{\partial}{\partial t} \rightarrow \frac{\partial}{\partial t} + \frac{\partial}{\partial z^*} \frac{\partial z^*}{\partial t}, \quad \frac{\partial}{\partial t} = \frac{\partial}{\partial t} - \frac{z^* u_H}{H} \frac{\partial}{\partial z^*} \quad (16)$$

where u_H is the velocity at which the bed height (interface between the three-phase fluidized zone and the two-phase non-fluidized zone) is moving, and is calculated as

$$u_H = \frac{dH}{dt} \quad (17)$$

For example, Eq. (2) (phase mass balance equation) can be rewritten in a dimensionless form as

$$\begin{aligned} \partial \frac{\varepsilon_k \rho_k}{\partial t} = & -\frac{1}{H} \left(\partial \frac{\varepsilon_k \rho_k U_k}{\partial z^*} - z^* u_H \partial \frac{\varepsilon_k \rho_k}{\partial z^*} \right) \\ & + \frac{1}{H^2} \frac{\partial}{\partial z^*} \left(D_{zk} \partial \frac{\varepsilon_k \rho_k}{\partial z^*} \right) + \sum_{i,j} T_{ik} \end{aligned} \quad (18)$$

The backward finite difference method (BFDM) was used to solve the partial differential equations (PDEs). Using second-order BFDM over a uniform grid of 20 intervals resulting in 3307 equations and 1026 differential variables. The total CPU time required to solve the case study described in the following section is about 80 s on a 800 MHz Pentium IV PC.

4. Results and discussion

The AFBR model is sensitive to the reactor organic load policy. Therefore, simulations of biological and hydrodynamic transients for a simple case study based on a low substrate concentration are here analyzed. The following specifications for reactor feed, fluidized bed reactor and inert support particles are assumed. As case study, a synthetic substrate with a concentration of 1 g COD L⁻¹ (70% glucose, 20% acetate and 10% milk powder) is fed to the bioreactor at a flow rate of 3.20 L d⁻¹. The reactor column has a maximum height H_{max} of 2.00 m, and a diameter D_c of 0.065 m. The static bed height H_0 is 0.70 m. The loaded support material ($W=3.50$ kg) has a density ρ_p of 2630 kg m⁻³, and a particle diameter d_p of 0.35 mm.

Model predictions considering ideal plug flow ($D_{zk}=0$), ideal perfect mixture ($D_{zk} \rightarrow \infty$) and non-ideal flow ($D_{zk} > 0$) patterns for the phases are analyzed. The liquid phase dispersion coefficient calculated by Eq. (15) is $D_{zL} = 1.83 \times 10^{-3} \text{ m}^2 \text{ s}^{-1}$ at the beginning of the

biological transient, and a decrease of 2.35% is computed along the process due to an increase of the biofilm concentration. Independently of the gas and solid phase dispersion coefficient values, the species concentrations in the liquid phase present approximately uniform profiles for these D_{zL} values. The gas ($k=G$) and solid ($k=S$) phase dispersion coefficients are ranged from $D_{zk}=0$ to $D_{zk}=0.2D_{zL}$. $D_{zG}=0.1D_{zL}$ and $D_{zS}=0.1D_{zL}$ values assure uniform concentration profiles in the solid phase. Gas phase presents a plug flow behavior for all tested dispersion coefficient values. Hereafter, the flow condition corresponding to $D_{zG}=0.1D_{zL}$, $D_{zS}=0.1D_{zL}$ and D_{zL} calculated by Eq. (15), is named as “totally dispersive” flow condition.

Following, Sections 4.1 and 4.2 show AFBR model predictions during hydrodynamic and biological transients, respectively. A sensitivity analysis of the reactor performance related to model parameters with high uncertainty is presented in Section 4.3. Finally, a second modeling approach considering a new control volume for extending the model to the non-fluidized bioreactor zone is presented in Section 4.4.

4.1. Hydrodynamic transient simulations

Fig. 5 shows the bed height profile for totally dispersive flow condition; both hydrodynamic and biological transient profiles are depicted. For a reactor inlet velocity U_0 of $1.81 \times 10^{-2} \text{ m s}^{-1}$, the time predicted to reach the hydrodynamic steady state condition departing from the static bed condition is approximately 4.50×10^{-4} days (39 s). This behavior is qualitatively the same for any (ideal and non-ideal) flow conditions of the phases in the reac-

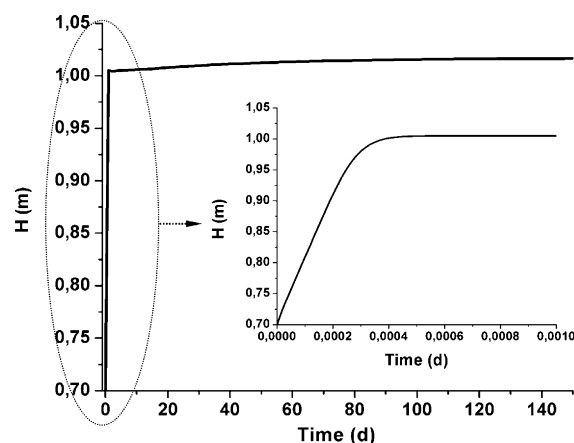


Fig. 5. Bed height (H) profile during the hydrodynamic and biological transients.

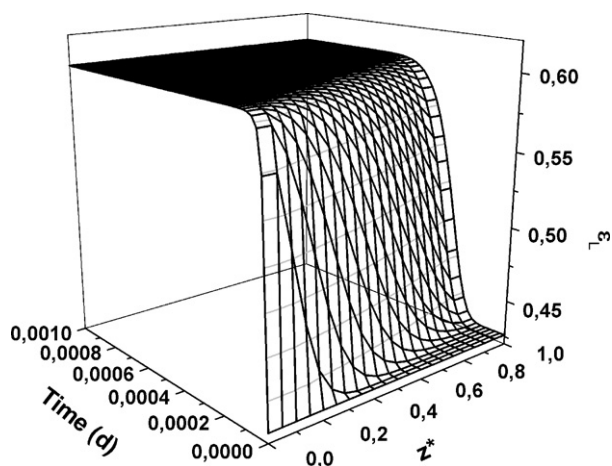


Fig. 6. Liquid holdup (ϵ_L) profile during the hydrodynamic transient.

tor. From ideal plug flow to complete mixture flow, a little lag to reach the steady state condition is computed.

Bed expansions around 45% are reached during the hydrodynamic transient. Fig. 6 depicts the liquid holdup profile corresponding to the bed height increase represented inside Fig. 5. In order to have the maximum superficial area available for biofilm attachment and prevent particle agglomeration, the bed porosity ϵ is set at $\epsilon \approx \epsilon_L \approx 0.60$ (Andrews & Trapasso, 1985).

Solid phase velocity is practically zero when compared to the liquid and gas ones (approx. $U_L = 3.01 \times 10^{-2}$ and $U_G = 1.45 \times 10^{-2} \text{ m s}^{-1}$) at the hydrodynamic steady state. Fig. 7 represents the solid phase velocity profile for totally dispersive flow condition during the hydrodynamic transient (axial dimensionless length z^* and time edges have been turned over with respect to Fig. 6).

4.2. Biological transient simulations

Independently of the phase dispersion coefficient values, the largest changes on the hydrodynamic properties evidently occur during the hydrodynamic transient as shown in Fig. 5 for the bed height.

Changes in the porosity of fluidized bed bioreactors due to biofilm development or biofilm detachment are less significant compared to changes in the height of the bed (Abdul-Aziz &

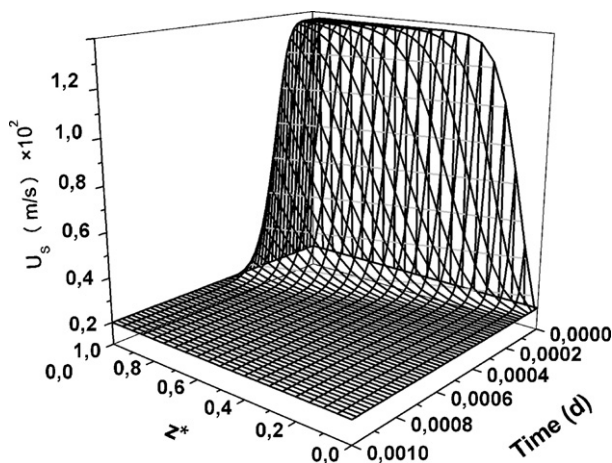


Fig. 7. Solid phase velocity (U_s) profile during the hydrodynamic transient.

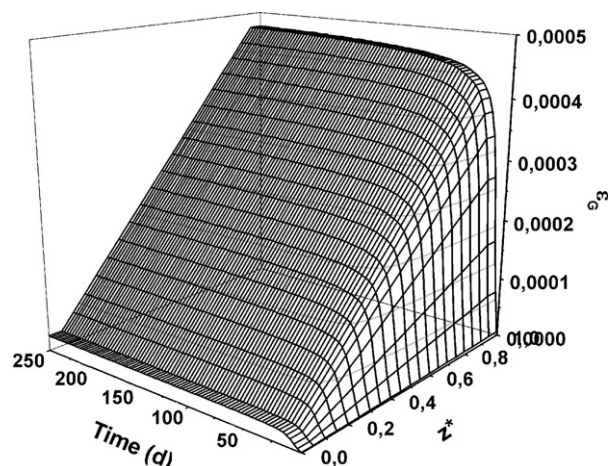


Fig. 8. Gas phase holdup (ϵ_G) profile during the biological transient.

Asokelar, 2000; Setiadi, 1995). Indeed, variations of approximately 0.12% and 1.25% in the bed porosity and height, respectively, for totally dispersive flow condition are predicted during the biological transient. Very similar results were obtained for the ideal plug flow pattern.

Because of the low COD concentration of the reactor feed, expected biomass and biogas yields are too low (Figs. 9 and 10). For this case study, as shown in Fig. 8, the gas phase holdup profile is practically negligible from a hydrodynamic point of view. Therefore, most published works assume AFBRs as solid–liquid two-phase systems to describe their hydrodynamics.

An increase in biofilm concentration or thickness makes bioparticles be fluidized in a greater extension due to a decrease in their specific density. Although the solid phase velocity is almost zero when the fluidized bed reaches the hydrodynamic steady state, a variation in this property is calculated while the biofilm concentration reaches the biological steady state condition. In the same way, the liquid phase velocity decreases slightly due to the biofilm concentration increment for all model predictions during the biological transient.

As expressed above and shown in Fig. 9, different biofilm concentration profiles are obtained depending on the phase dispersion coefficient values. A decrement of 20% in the biofilm concentration in the bed axial direction is predicted instead of using a plug flow model (Fig. 9(b)). Glucose acidogenic degraders and acetoclastic methanogens are the species present in the largest proportions. As 70% of the total COD fed is provided by glucose, a high concentration of glucose acidogenic degraders is predicted at the reactor inlet, where the substrate concentration is high. Thus, glucose acidogenic degraders determine the characteristics of the biofilm concentration profile.

Even though substrate concentration remains almost constant after 40 days, the microorganisms concentration in liquid and solid phases varies because of the combination of detachment processes and maintenance of microorganisms due to the contribution of the soluble substrate (glucose, fatty acids and amino acids) produced during the hydrolysis of non-active biomass. The biological steady state condition is approximately reached at day 250 (Fig. 9).

A characteristic pH decrease is observed during the first days because of a faster glucose degradation rate to VFAs when compared with the consumption rates of the subsequent biological stages. The pH stability can be attributed to the carbonate/bicarbonate buffering produced by the generation of CO_2 in the digestion process, which is not completely removed from the reactor as gas. Fig. 10

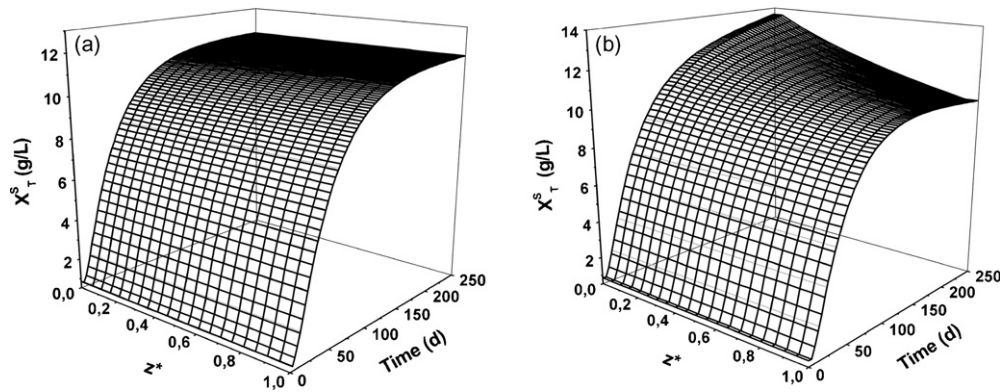


Fig. 9. Biofilm concentration (X_T^S) profile for: (a) totally dispersive flow condition, (b) plug flow condition.

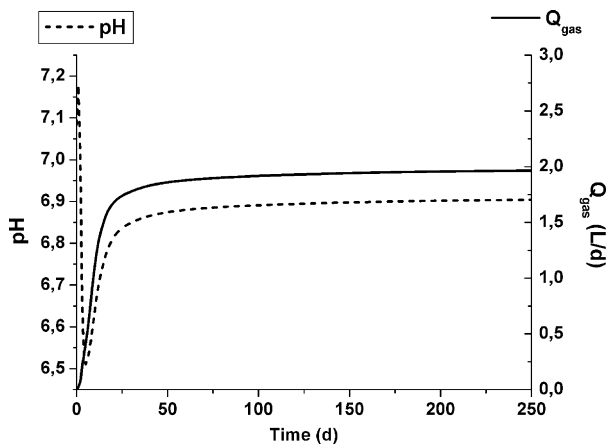


Fig. 10. pH and generated biogas flow (Q_{gas}) profiles.

represents the pH and generated biogas flow profiles for the totally dispersive flow condition.

Simulation results allow studying the system in view to control. For example, for this case study, the COD removal efficiency reaches approximately 80% at day 40 (84% at the steady state, day 250) (Fig. 11). At this time, it could be a good decision to carry out a change in the organic load attending to the long period for recovering a biological steady state regimen. Thus, an optimal organic

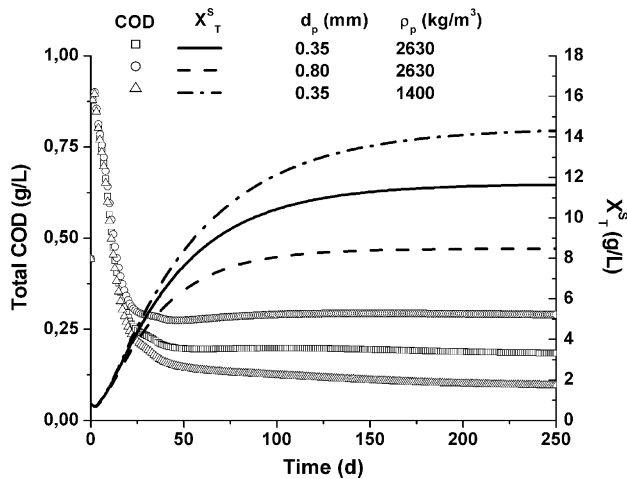


Fig. 11. Biofilm concentration and total COD during the biological transient for the original case study and scenarios (a) and (b).

load policy guarantees the best reactor performance in the shortest period of time. The model is able to resist strong numerical disturbances to represent a “step by step” start up of the reactor. So, the organic load policy optimization could be one main application of the AFBR model. Generally, industrial processes follow cyclical production patterns established by plant operating schedules or periodical domestic sewage disposals. The bioreactor model allows evaluating effluent treatment systems following “real” flow patterns.

4.3. Sensitivity analysis of model predictions related to model parameters

The specific biofilm detachment rate and the liquid–gas mass transfer coefficient are the model parameters with the highest uncertainty. Characteristics (diameter and density) of the inert support particles are also very important because of their influence in the specific surface area for biofilm attachment and bed fluidization characteristics.

The biological steady state is sensitive to the specific biofilm detachment rate ($k_E = 2.24 \times 10^{-10} \text{ m s}^2 \text{ kg}^{-1}$). An increase of 50% in k_E predicts a decrease of 12% in the biofilm concentration and a decrease in the time required to reach the biological steady state. On the contrary, a decrease in k_E predicts an increase in the biofilm concentration and therefore, an increase in the total COD removal efficiency.

Because of the effect of the mass transfer coefficient $k_L a$ on system pH and partial pressures of gas phase components, a decrease in $k_L a$ predicts a decrease in the system pH and, thus, a decrease in the biofilm concentration and biogas production.

Assuming spherical geometry, the superficial area for biofilm attachment and the particle characteristics at static bed condition are related as follows:

$$A_p^T = N_p A_p = \left(\frac{V_p^T}{V_p} \right) A_p = \frac{6}{d_p} V_p^T = \frac{6}{d_p} \left(\frac{W}{\rho_p} \right) = \frac{6}{d_p} V_o \varepsilon_{S_o} \quad (19)$$

where A_p , A_p^T , V_p , V_p^T are the particle and total superficial area and volume, respectively; N_p is the number of particles, and subscript o refers to static bed condition. From Eq. (19), it is observed that: (a) keeping constant particle density using the same support material, a change in the particle diameter causes a change in the superficial area for biofilm attachment for the same initial total solid volume ($V_p^T = V_{S_o}$), i.e. the same solid holdup ε_{S_o} and bed volume V_o ; (b) keeping the same particle diameter but using different support material (different particle density), it is possible to maintain the superficial area and the initial total solid volume by changing the support particle load W . Based on scenarios (a)

and (b), the effect of the inert support particle characteristics on the bioreactor performance is analyzed. Uniform profiles (totally dispersive flow condition) of the biofilm concentration and total COD during the biological transient for scenarios (a) and (b) are compared to the original case study in Fig. 11.

A particle diameter d_p of 0.80 mm is selected for scenario (a). An increase in the fluid velocity at the reactor inlet ($U_o = 4.58 \times 10^{-2} \text{ m s}^{-1}$) and 2.00×10^{-4} days (18 s) are necessary to obtain equal initial fluidization characteristics as shown in Fig. 5. However, lower attached biomass concentration values than those of the original case are observed during the biological transient (Fig. 11). This is explained by a decrease in the biofilm attachment area and an increase in the detachment rate for the same specific detachment rate coefficient k_E .

The same particle diameter and a lower support material density ($\rho_p = 1400 \text{ kg m}^{-3}$) with respect to the original case are assumed for scenario (b). Because of a lower particle density, the fluid velocity at the reactor inlet has to be diminished ($U_o = 5.05 \times 10^{-3} \text{ m s}^{-1}$) to obtain equal fluidization characteristics as shown in Fig. 5 during the hydrodynamic transient of 1.00×10^{-3} days (86 s). Even when the superficial area for biofilm attachment is the same as that of the original case, increments in the attached biomass concentration are observed during the biological transient because of the decrease in the detachment rate caused by a lower inlet fluid velocity U_o and a lower fluid pressure gradient (Fig. 11).

The relationship between biofilm thickness and attached biomass concentration is strongly dependent on the bioparticle model assumed. Biofilm thickness steady state values of 0.66, 1.08 and $0.80 \mu\text{m}$ are reached for the original case study and scenarios (a) and (b), respectively. In this work, a spherical geometry and homogeneous biofilm distribution on the inert support particles are assumed. The biofilm is non-homogeneously distributed on the real support particles. It depends on particle characteristics (shape, roughness, material porosity, size and weight) and on the hydrodynamic conditions, such as the fluid erosion on the bioparticle surface. By scanning electron microscope (SEM) it was observed that microorganisms are attached to approximately 50% of the superficial area of sand particles, mainly covering the deep zones of the particles due to abrasion and erosion effects on the exposed zones (Mussati, Thompson, Fuentes, Aguirre, & Scenna, 2005b). This means that if a more realistic bioparticle model is included in the bioreactor model, a closer correspondence between the total (active and non-active) attached biomass concentration and biofilm thickness values is obtained. It will be a motivation for a future work.

Different total COD levels due to the ongoing microbiological processes and hydrodynamics determine different reactor efficiencies. Although these are theoretical results, the sensitivity analysis of model results related to inert support characteristics shows a trade-off between operating costs (e.g. support material and pumping) and treatment efficiencies.

4.4. About the control volume to be assumed

Up to then, the AFBR model has been solved considering the three-phase fluidized bed zone as control volume. Following, it will be extended to the two-phase non-fluidized bed zone for evaluating the effect of the substrate consumption by suspended biomass in this bioreactor zone. This assumption implies modeling a gas-liquid reactor in the non-fluidized zone of the reactor column limited by fluidized bed height and the maximum column height ($H < z \leq H_{\text{max}}$), in principle, considering ideal plug flow conditions. All mass and momentum balance equations described in Section 2 are valid if considering the solid phase holdup being equal to zero ($\epsilon_s = 0$).

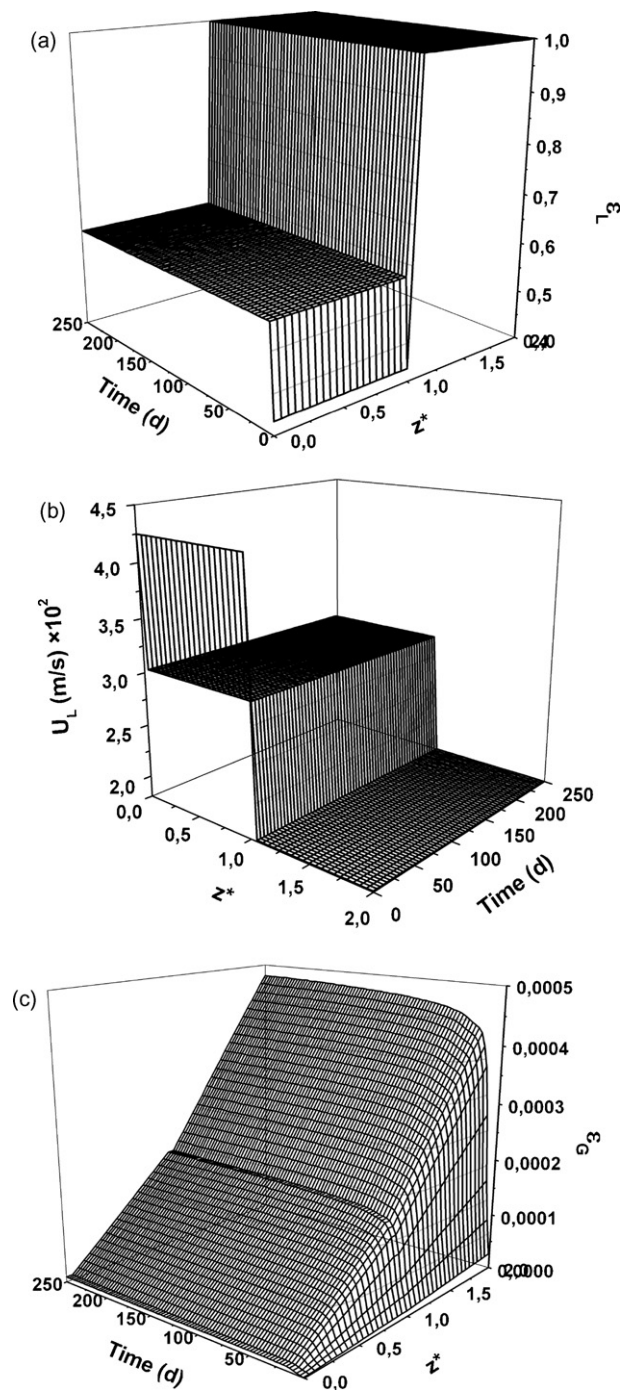


Fig. 12. Properties of the whole reactor column ($0 \leq z^* \leq 2$): (a) Liquid phase holdup (ϵ_L), (b) Liquid phase velocity (U_L), and (c) gas phase holdup (ϵ_G).

Eq. (20) couples the heights of the fluidized and non-fluidized bed zones, hereafter named H_f and H_{nf} , respectively.

$$H_{\text{max}} = H_f + H_{nf} \quad (20)$$

The axial dimensionless length z^* is defined as $1 < z^* \leq 2$ for the non-fluidized zone. From Eq. (20), the relationship among the velocities at which heights H_f and H_{nf} are moving has to verify (see Eq. (17)):

$$u_{H_f} = -u_{H_{nf}} \quad (21)$$

and as for the fluidized zone, the derivatives of the variables that are functions of z in the non-fluidized zone must be rewritten as

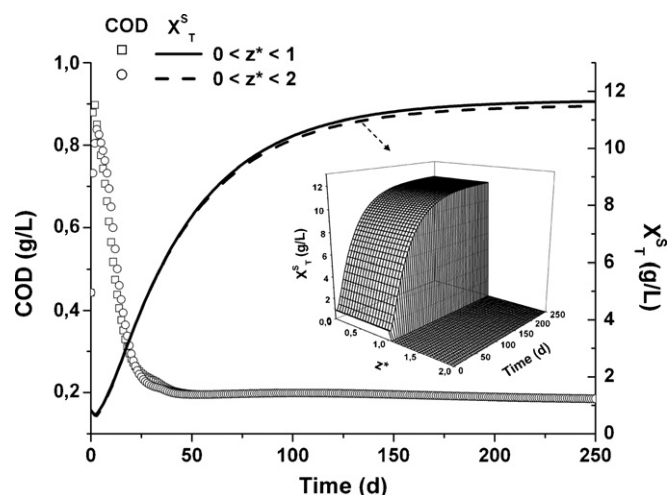


Fig. 13. Biofilm concentration (X_T^S) profiles (original case study) for different control volumes.

follows:

$$\frac{\partial}{\partial z} = \frac{1}{H_{nf}} \frac{\partial}{\partial z^*} \quad \text{and} \quad \frac{\partial}{\partial t} = \frac{\partial}{\partial t} - \frac{z^* u_{H_{nf}}}{H} \frac{\partial}{\partial z^*}$$

The liquid phase holdup and velocity, and gas phase holdup of the whole bioreactor column ($0 \leq z^* \leq 2$) are depicted in Fig. 12(a), (b) and (c), respectively, for the original case study described in Section 4 (totally dispersive flow condition). As shown in Fig. 12(a), $\epsilon_L \approx 1$ in the non-fluidized zone because the gas holdup also represents a little fraction of control volume in this zone (Fig. 12(c)); and the liquid phase velocity reaches almost the same values of the flow velocity at the reactor inlet U_0 (Fig. 12(b)).

The extended model predictions present a deviation of 1.42% in the biofilm concentration compared to the results obtained from the application of the AFBR model to the three-phase fluidized zone. As shown in Fig. 13, the substrate consumption not only by attached and suspended microorganism in the fluidized zone, but also by the suspended ones in the non-fluidized zone, causes a little decrease in the attached biomass concentration. However, for this case study the effect is so little that COD concentration is practically the same for both approaches (Fig. 13).

The effect of the substrate consumption by suspended biomass in the non-fluidized zone depends on some operational and reactor design factors such as: the biomass concentration which is a function of the biofilm detachment rate, the H_f/H_{nf} ratio, and the substrate residence time. The influences of these factors were evaluated for different scenarios (results not shown). For example, a decrease of 3.60% and 0.24% are calculated in the biofilm concentration for scenarios (a) and (b) described in Section 4.3, respectively. In all cases, an important decrease in the biofilm concentration affects the COD removal efficiency.

From a numerical point of view, modeling of hypothesis that considers biochemical transformations occur in the fluidized bed zone and in both the free-support material zone requires a higher programming effort and duplicates the number of equations. Using the BFD method of second order over a uniform grid of 40 intervals for keeping the step length in the bed axial direction ($0 \leq z^* \leq 2$), as similar as the above solution (20 intervals in $0 \leq z^* \leq 1$), the equation and differential variables numbers rise to 6535 and 1785, respectively, and the total CPU time is about 200 s (see Section 3).

The choice of the control volume to apply and solve the AFBR model will depend on the precision with the processes need to be described.

5. Conclusions

The global model (bioprocesses and hydrodynamics) here proposed neglects the internal mass transfer phenomena, and allows to evaluate the anaerobic digestion in the context of the fluidized bed reactor configuration, focused on dynamics of solids (bioparticles) and effects of hydrodynamic events on biofilm development. Model allows calculating variation of properties along the axial direction of the bed, including bed stratification and changes in the particle characteristics.

For a case study, and based on the simulation results, both biological and hydrodynamic behaviors of an AFB reactor were investigated. Bioreactor performance was analyzed through the profiles of the main variables such as phase holdup and velocity, pH, biomass concentration and generated biogas flow. Based on the results obtained during this study, the following conclusions can be drawn:

1. Besides the phase dispersion coefficients, the specific detachment rate k_E and liquid-gas mass transfer coefficient $k_L a$ are the model parameters with the highest uncertainties. Depending on phase dispersion coefficient values (different flow conditions), different biomass concentration profiles were obtained along the axial direction of the bed. An increase in k_E causes a decrease in the biofilm concentration and in the time required to reach the steady state condition. A decrease in $k_L a$ predicts a decrease in the system pH and, thus, in the biofilm concentration and biogas production.
2. The effect of the support particle characteristics (particle density and diameter) on the biofilm processes and the bed fluidization was studied. An increase in the particle diameter or density requires an increase in the fluid velocity at the reactor inlet to maintain equal initial fluidization characteristics, and predicts lower attached biomass concentration values during the biological transient.
3. The fact of considering the whole column volume as the control volume allowed evaluating the effect of substrate consumption by suspended biomass in the free-bioparticles zone of the bioreactor. In the case studies here presented, a decrease in the biofilm concentration up to 3.6% was observed. However, some factors involving the biofilm detachment rate, reactor design characteristics and substrate residence time need to be analyzed for each specific case. The implementation of this modeling approach involved a higher programming effort and a longer CPU time.

The model can be straightforward extended to different substrate degradation schemes. Since biomass development, and thus the bioreactor efficiency, is affected by feed composition and evolution of operational conditions, there are two broad areas of application for this model: theoretical and practical. An example of theoretical application is the prediction of intermediates not easily measurable. Practical applications include on-line prediction, reactor design and optimization, hydraulic design, control strategies evaluation, and start up optimization, among others.

Acknowledgements

Financial support from Consejo Nacional de Investigaciones Científicas y Técnicas (CONICET), Agencia Nacional para la Promoción de la Ciencia y la Tecnología (ANPCyT) and Universidad Nacional del Litoral of Argentina is acknowledged.

References

- Abdul-Aziz, M. A., & Asokelar, S. R. (2000). Modeling of biological particle mixing in a fluidized-bed biofilm reactor. *Water Environment Research*, 72, 105–115.
- Andrews, G., & Trapasso, R. (1985). The optimum design of fluidized bed bioreactors. *Journal of Water Pollution Control Federation*, 57(2), 143–150.
- Angelidaki, I., Ellegaard, L., & Ahring, B. K. (1999). A comprehensive model of anaerobic bioconversion of complex substrates to biogas. *Biotechnology and Bioengineering*, 63(5), 363–372.
- Batstone, D. J., Keller, J., & Blackall, L. L. (2004). The influence of substrate kinetics on the microbial community structure in granular anaerobic biomass. *Water Research*, 38, 1390–1404.
- Batstone, D. J., Keller, J., Angelidaki, I., Kalyuzhnyi, S. V., Pavlostathis, S. G., Rozzi, A., Sanders, W. T. M., Siegrist, H., & Vavilin, V. A. (2002). *Anaerobic Digestion Model No. 1 (ADM1) IWA Task Group for mathematical modelling of anaerobic digestion processes*. London, UK: IWA Publishing.
- Bonnet, B., Dochain, D., & Steyer, J. P. (1997). Dynamical modelling of an anaerobic digestion fluidized bed reactor. *Water Science and Technology*, 36(5), 285–292.
- Diez Blanco, V., García Encina, P. A., & Fdez-Polanco, F. (1995). Effects of biofilm growth, gas and liquid velocities on the expansion of an anaerobic fluidized bed reactor (AFBR). *Water Research*, 29(7), 1649–1654.
- Foscolo, P. U., & Gilibaro, L. G. (1987). Fluid dynamic stability of fluidized suspensions: the particle bed model. *Chemical Engineering Science*, 42(6), 1489–1500.
- Foscolo, P. U., Gilibaro, L. G., & Waldarm, S. P. (1983). A unified model for particulate expansion of fluidized beds and flow in fixed porous media. *Chemical Engineering Science*, 38(8), 1251–1260.
- Fuentes, M., Aguirre, P., Scenna, N., & Mussati, M. (2007). Anaerobic digestion of carbohydrate and protein-based wastewaters in fluidized bed bioreactors. *Latin American Applied Research*, 37(4), 235–242.
- Fuentes, M., Aguirre, P., Scenna, N., & Mussati, M. (2008). Anaerobic biofilm reactor modeling focused on hydrodynamics. *Chemical Engineering Communications*, 195(6), 600–621.
- Graef, S. P., & Andrews, J. (1973). Mathematical modeling and control of anaerobic digestion. *AIChE Symposium Series*, 70(136), 101–131.
- Hatta, N., Fujimoto, H., Isobe, M., & Kang, J. (1998). Theoretical analysis of flow characteristics of multiphase mixtures in a vertical pipe. *International Journal of Multiphase Flow*, 24(4), 539–561.
- Hermanowicz, S. W., & Ganzarczyk, J. J. (1983). Some fluidization characteristics of biological beds. *Biotechnology and Bioengineering*, 25, 1321–1330.
- Huang, J., & Wu, C. (1996). Specific energy dissipation rate for fluidized bed bioreactors. *Biotechnology and Bioengineering*, 50, 643–654.
- Huang, J., Yan, J., & Wu, C. (2000). Comparative bioparticle and hydrodynamic characteristics of conventional and tapered anaerobic fluidized-bed bioreactors. *Journal of Chemical Technology and Biotechnology*, 75, 269–278.
- Kim, S. D., & Kim, C. H. (1983). Axial dispersion characteristics of three phase fluidized beds. *Journal of Chemical Engineering of Japan*, 16, 172–178.
- Mulcahy, L. T., & Shieh, W. K. (1987). Fluidization and reactor biomass characteristics of the denitrification fluidized bed biofilm reactor. *Water Research*, 21, 451–458.
- Muroyama, K., & Fan, L. S. (1985). Fundamentals of gas–liquid–solid fluidization. *AIChE Journal*, 31, 1–34.
- Mussati, M., Fuentes, M., Aguirre, P., & Scenna, N. (2005). A steady-state module for modeling anaerobic biofilm reactors. *Latin American Applied Research*, 35, 255–263.
- Mussati, M., Thompson, C., Fuentes, M., Aguirre, P., & Scenna, N. (2005). Characteristics of a methanogenic biofilm on sand particles in a fluidized bed reactor. *Latin American Applied Research*, 35, 265–272.
- Ngian, K.-F., & Martin, W. B. (1980). Bed expansion characteristics of liquid fluidized particles with attached microbial growth. *Biotechnology and Bioengineering*, 22, 1843–1856.
- Nicolella, C., van Loosdrecht, M. C. M., & Heijnen, S. J. (2000). Particle-based biofilm reactor technology. *Trends in Biotechnology*, 18(7), 312–320.
- Process System Enterprise Ltd. (2004a). gPROMS Advanced User Guide, Release 2.3, London.
- Process System Enterprise Ltd. (2004b). gPROMS Introductory User Guide, Release 2.3.1, London.
- Richardson, J. F., & Zaki, W. N. (1954). Sedimentation and fluidization. Part 1. *Transactions on the Institute of Chemical Engineers*, 32, 35–53.
- Setiadi, T. (1995). Predicting the bed expansion of an anaerobic fluidized bed bioreactor. *Water Science and Technology*, 31, 181–191.
- Thomas, C. R., & Yates, J. G. (1985). Expansion index for biological fluidized beds. *Journal of Institute of Chemical Engineers*, 63, 67–70.
- Yu, H. Q., & Rittmann, B. E. (1997). Predicting bed expansion and phase holdups for three-phase fluidized-bed reactors with and without biofilm. *Water Research*, 31(10), 2604–2616.
- Yu, H. Q., & Fang, H. H. P. (2003). Acidogenesis of gelatin-rich wastewater in an upflow anaerobic reactor: influence of pH and temperature. *Water Research*, 37, 55–66.